ACS APPLIED MATERIALS & INTERFACES

Research Article

www.acsami.org

Thermal Decomposition of Bismuth Oxysulfide from Photoelectric Bi_2O_2S to Superconducting $Bi_4O_4S_3$

Xian Zhang,[†,‡] Yufeng Liu,[‡] Ganghua Zhang,[‡] Yingqi Wang,[§] Hui Zhang,*[,‡] and Fuqiang Huang*[,†,‡]

[†]Beijing National Laboratory for Molecular Sciences and State Key Laboratory of Rare Earth Materials Chemistry and Applications, College of Chemistry and Molecular Engineering, and [§]Department of Material Science and Engineering, College of Engineering, Peking University, Beijing 100871, China

[‡]CAS Key Laboratory of Materials for Energy Conversion and State Key Laboratory of High Performance Ceramics and Superfine Microstructure, Shanghai Institute of Ceramics, Chinese Academy of Sciences, Shanghai 200050, P. R. China

Supporting Information

ABSTRACT: With the addition of oxygen into the chain-like bismuth sulfide of Bi_2S_3, there are two interesting functional compounds of Bi_2O_2S (photoelectric) and $Bi_4O_4S_3$ (superconducting) containing the PbO-like $[Bi_2O_2]$ layers. Nanoscale Bi_2O_2S crystals with an indirect band gap of 1.12 eV are synthesized via a facile hydrothermal method. This semiconductor shows excellent photoelectric response under the irradiation of visible light lamp at room temperature. Theoretical calculations and packing factor model both indicate that the loosely packed Bi_2O_2S is an excellent photoelectric material. When the Bi_2O_2S phase was annealed at 500 °C in an evacuated quartz tube, nanocrystals of $Bi_4O_4S_3$ were obtained. The powder X-ray diffraction and electron microscope analyses (SEM, TEM, EDX) confirmed the thermal decomposition from orthorhombic Bi_2O_2S to tetragonal $Bi_4O_4S_3$. The superconducting transition temperature of $Bi_4O_4S_3$ was observed to be 4.6 K from the temperature-dependence measurements of electrical resistivity and magnetic susceptibility. Our results also provide a new method utilizing thermal decomposition to prepare a new phase without high temperature reaction.

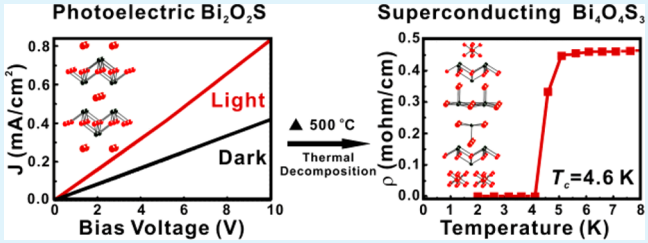

KEYWORDS: *bismuth oxysulfide, photoelectric, superconductor, thermal decomposition*

INTRODUCTION

PbO-like $[Bi_2O_2]$ layers have attracted enormous attention because of their presence in many important compounds, such as ferroelectric materials ($SrBi_2Ta_2O_9$),[1] famous photocatalysts BiO*X* (X = Cl, Br, I),[2−4] BiOCuS-based superconductor,[5−7] recently discovered superconductors $Bi_4O_4(SO_4)_{0.5}Bi_2S_4$,[8−10] and so on. Similar to the structure of PbO, the $[Bi_2O_2^{2+}]$ layer can be considered as corner-sharing tetrahedra $[OBi_4]$ whose O atoms are located at the nodes of a square net, as shown in Figure 1. BiOCl and its halide relatives possess excellent photocatalytic properties, which was reported to be superior to nanotitania.[2] BiOCuS is composed of the alternating layers of $[Bi_2O_2]$ and $[Cu_2S_2]$,[5] and $Bi_4O_4S_3$ consists of $[Bi_2O_2]$ layers, $[BiS_2]$ layers, and SO_4^{2-} anions,[9] the compounds exhibit superconductivity without any ions doping. $Bi_4O_4S_3$ may be another fascinating superconductor after FeSe[11,12] and offered a simplified model for theoretical and experimental studies.

BiOCl is an excellent photocatalyst, but only functions under the UV-light irradiation. Fortunately, BiOBr and BiOI can be driven by visible light, but suffer more severely from the photo decomposition under solar light. Nanosized Bi_2O_3 has a slightly too large light absorption edge (E_g = 2.8 eV) for absorbing visible light.[13−15] Bi_2S_3 has a smaller band gap of 1.3 eV but the chemical stability is also very poor.[14] There is another $[Bi_2O_2]$-contained compound Bi_2O_2S,[16,17] whose crystal structure is similar to BiO*X*. Only one column of S^{2-} anions separates two $[Bi_2O_2]$ layers in Bi_2O_2S, compared with two columns of Cl^- anions in BiO*X*. Such different arrangements are due to different manners of charge balance. The presence of S atoms between the $[Bi_2O_2]$ layers not only narrows down the band gap of BiOCl but also stabilizes the material during photocatalysis. Few investigations have been performed on Bi_2O_2S except one on photocatalysis and photochemical cells.[17] The band gap of Bi_2O_2S (E_g = 1.5 eV) may be too small for water splitting. But Bi_2O_2S is suitable to act as a photovoltaic light absorber material in solar cells due to its favorite E_g around 1.5 eV. Furthermore, the compound has a very loosely packed structure with a packing factor (PF) of 0.66 calculated from the packing factor model, which is used for selecting good photocatalysts and photovoltaic materials.[2,18] Therefore, Bi_2O_2S may be a good photovoltaic material.

These $[Bi_2O_2]$-contained materials are mainly prepared from the solid-state high temperature reactions, which have to undergo complex mechanical grinding and repeated sintering process for a long time, and some impurities are usually unavoidable. Therefore, it is necessary to exploit facile synthetic

Received: December 30, 2014
Accepted: February 3, 2015
Published: February 3, 2015

DOI: 10.1021/am5092159
ACS Appl. Mater. Interfaces 2015, 7, 4442−4448

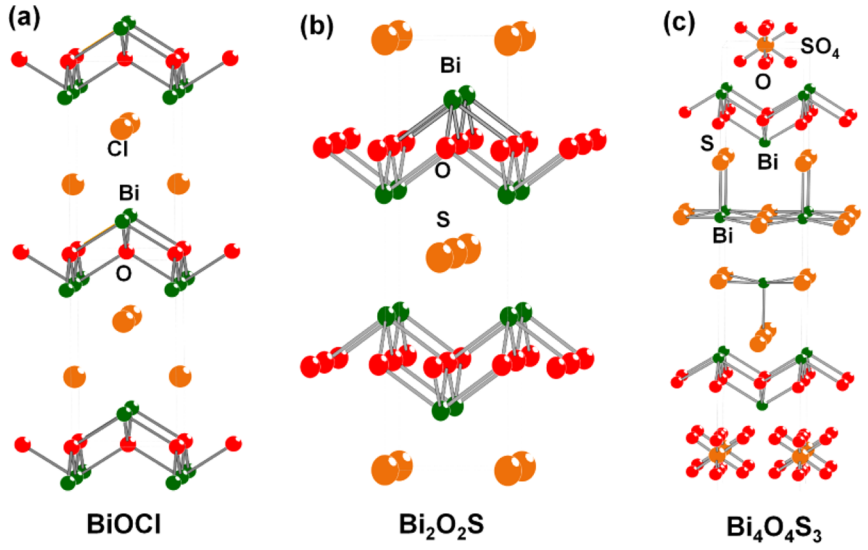

Figure 1. Crystal structures viewed down along (100): (a) BiOCl, (b) Bi_2O_2S, and (c) $Bi_4O_4S_3$. For clarity, the chemical bonds to $[Bi_2O_2]$ layer and one-half cell of $Bi_4O_4S_3$ are not presented in the figure.

methods. Commonly, single-crystal to single-crystal transformations are amazing phenomena, with which theoretical and experimental researchers can adjust the functions of the materials possessing these properties. In fact, extensive efforts have been devoted to the thermal decomposition studies for various compounds to achieve the switch of some unique functions. Therefore, the thermal decomposition can be a new strategy for the preparation of BiS_2-based superconductors. Because of the similar chemical component and notable photoelectric response, Bi_2O_2S is a suitable candidate for the research of thermal decomposition to the superconducting $Bi_4O_4S_3$.

In this work, we present a feasible way to transform the light-absorbing Bi_2O_2S to superconducting $Bi_4O_4S_3$. For its advantages of the mild reaction conditions, convenient operation process, easy handling and simple apparatus usage, hydrothermal method has been demonstrated as a feasible route to obtained superconductor compounds and numerous sulfides with high purity and phase homogeneity. Thus, Bi_2O_2S nanocrystals were synthesized via a facile hydrothermal method with uniform size and good crystallinity and their excellent photoelectric properties were achieved. Theoretical analyses were performed to explore the potential of photoelectric effect in Bi_2O_2S. Superconducting $Bi_4O_4S_3$ was obtained via a convenient route by directly annealing Bi_2O_2S nanocrystals. The thermal decomposition offers a novel route to synthesizing other superconductors and functional materials.

EXPERIMENTAL SECTION

Synthesis of Nanoscale Bi_2O_2S Crystals. Ten milliliters of deionized water, 4 mmol of $Bi(NO_3)_3{\cdot}5H_2O$, and 3 mmol of CH_4N_2S were added into a 50 mL beaker to form an orange solution under stirring. Afterward, 12 g of $LiOH{\cdot}H_2O$ powder was added gradually into the beaker to form a black mixture under stirring for 10 min. Finally, the reaction mixture was then transferred into a 50 mL Teflon-lined stainless steel autoclave with 75% filling. The crystallization process was carried out under autogenous pressure at 200 °C for 3 days. After the autoclave was cooled and depressurized, the products was taken out and poured into 40 mL of deionized water, and centrifuged at 5000 rpm for 5 min. The precipitates were collected, washed three times by deionized water, and dried in an oven at 80 °C for 6 h.

Synthesis of $Bi_4O_4S_3$ Powders. One-half a gram of Bi_2O_2S nanocrystals were initially ground and pelletized subsequently in air. The pellets were sealed in an evacuated quartz tube and sintered at 500 °C for 6 h, and then the crystalline sample was obtained.

Characterization. Field-emission scanning electron microscopy (FESEM) images were acquired using a FEI Sirion 200 instrument with an energy dispersive X-ray (EDS) analysis capability. Low and high resolution transmission electron microscopy (TEM) images were taken on a JEOL JEM-2100F TEM at an accelerating voltage of 200 kV. The TEM samples were prepared by dip-casting Bi_2O_2S nanocrystals dispersed in ethanol onto carbon-coated copper TEM grids. X-ray diffraction (XRD) patterns were collected on a Bruker D8 Focus X-ray diffractometer equipped with a monochromatized source of Cu Kα radiation (λ= 0.15406 nm) at 1.6 kW (40 kV, 40 mA). The patterns were recorded in a slow-scanning mode with 2θ from 10° to 80° with a scan-rate of 6°/min. UV–vis-NIR absorbance spectra were recorded on a Hitachi U-4100 spectrophotometer with an scanning velocity of 240 nm/min. X-ray photoelectron spectroscopy (XPS) data were obtained using an ESCAlab250 X-ray Photoelectron Spectroscopy instrument for surface analysis. Photocurrent density–voltage (J–V) characteristics were measured under visible light with a 300 W xenon lamp (filter: λ = 420 nm). Magnetic properties were studied using a Quantum Design Physical Property Measurement system (PPMS). Temperature-dependent direct-current (DC) magnetic susceptibility (M-T) curve of the sample was measured from 300 to 2 K under 10 Oe magnetic field under zero-field cooling (ZFC) and field-cooling (FC) conditions.

Electronic Structure Calculation. The first-principles computations based on the density-functional theory (DFT) were performed using the WIEN2K program package.[19] The Perdew–Burke–Ernzerhof (PBE)[20] version of the generalized gradient approximation (GGA) was used to describe the exchange correlation function and the linearized augmented plane wave (LAPW) method (PAW)[21] method has been used in the present work. The atomic electron configuration for Bi treated 6s, 6p states as valence states, and the others were described by 2s, 2p valence states for O and 3s, 3p valence states for S and Cl, respectively. The cutoff energy of plane wave was chosen at 350 eV. For the structure optimizations, 6 × 6 × 6 Monkhorst–Pack grids were used for the primitive cell and 4 × 4 × 4 k-points for the conventional cell, respectively. The relaxation of geometry optimization was performed until the total energy changes within 1×10^{-6} eV/atom and the Hellmann–Feynman force on all atomic sites was less than 0.01 eV /Å.

DOI: 10.1021/am5092159
ACS Appl. Mater. Interfaces 2015, 7, 4442–4448

RESULTS AND DISCUSSION

Bi_2O_2S was prepared from a newly developed thiourea (CH_4N_2S) method. CH_4N_2S as a sulfur source gradually releases S at a relatively higher temperature of 200 °C than its melting point of 182 °C, while elemental sulfur in aqueous concentrated base (AOH; A = alkali metal ions) is commonly used to prepare sulfide compounds.[16] The previously reported samples were synthesized from Bi_2O_3 and Bi_2S_3 in 10% NaOH solution[16] or from Bi_2O_3 in Na_2S solution,[17] but the final product is not pure. The morphology of our Bi_2O_2S nanocrystals was characterized by FESEM and TEM, as shown in Figure 2. Bi_2O_2S single crystals have bricklike surface

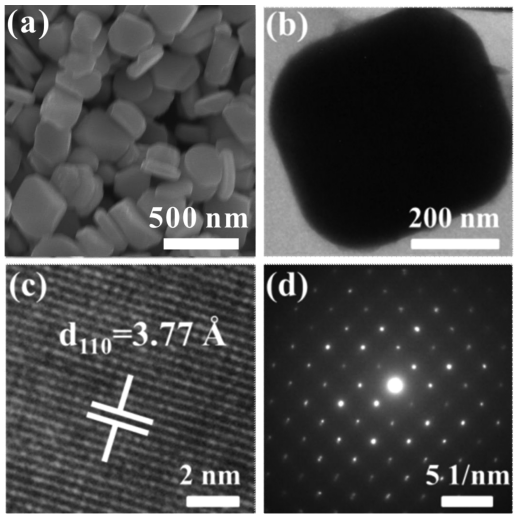

Figure 2. (a) FESEM of Bi_2O_2S nanocrystals, (b) TEM of an individual single crystal, (c) HRTEM of (110) spacing plane, (d) SAED of the single crystal.

and uniform size with an average size about 300 nm (Figure 2a, b), whose quality is much better than the previously reported one.[17] Clear lattice fringe of an individual Bi_2O_2S single crystal is observed in Figure 2c, which indicates that the single crystal has good crystallinity. The interplanar spacing of the single crystal is 3.77 Å corresponding to the (110) planes of Bi_2O_2S indexed with an orthorhombic structure. The SEAD of the individual Bi_2O_2S nanocrystal indicated that it is monocrystalline (Figure 2d).

The structure and phase purity of the Bi_2O_2S nanocrystals were confirmed by XRD patterns. The typical XRD pattern of Bi_2O_2S nanocrystals was indexed to the orthorhombic *Pnnm* space group,[16,17] as shown in Figure 3a. Diffraction peaks of Bi_2O_2S nanocrystals at 2θ = 14.9, 24.3, 27.5, 30.0, 32.3, 32.7, 33.8, 45.0, 45.6, 47.5, 50.8, 54.0, 55.3, 57.3, 58.5, 59.3, 61.6, 62.3, 69.3, and 72.5° correspond to (020), (110), (120), (040), (130), (101), (111), (141), (060), (002), (151), (112), (221), (161), (132), (170), (250), (080), (212), and (261) planes of the orthorhombic structure of Bi_2O_2S, respectively. The thiourea method can prepare pure sample, in contrast with the reported methods.[16,17] The UV−vis absorbance spectrum of Bi_2O_2S nanocrystals is shown in Figure 3b. The deep-red Bi_2O_2S nanocrystals absorb the light from ultraviolet to near-infrared region of 971 nm. For the indirect band gap semiconductor of Bi_2O_2S, the Kubelka−Munk absorbance is proportional to the square root of $(h\nu - E_g)$, that is $F \sim (h\nu - E_g)^{1/2}$,[22] where $h\nu$ is photon energy, E_g is the band gap of the material. Using this method, the optical band gap of Bi_2O_2S nanocrystals estimated to be ~1.12 eV by plotting $(\alpha h\nu)^{1/2}$ (the square of product of the absorption coefficient (α) and the photon energy ($h\nu$)) versus $h\nu$ as shown in Figure 3b insert. The E_g value is much smaller than the one previously reported of 1.5 eV. However, the reported sample is not pure from its XRD pattern and the absorption edge is very flat and not as sharp as that of our sample.[17] Therefore, our estimated of E_g should be more reliable than the reported one. EDX analysis of selected regions of the sample showed the presence of all three elements with a constant ratio, indicating a uniform composition of $Bi_{2.06}O_{2.03}S_{0.91}$ as depicted in Figure S1 in the Supporting Information, consistent with the expected formula. The dark-red appearance color of the Bi_2O_2S crystals may be due to the indirect band gap and relatively flat absorption edge, even though the E_g is rather small.

In order to confirm the oxidation state of Bi, O and S atoms, XPS measurement was carried out for the Bi_2O_2S sample (Figure 4) and for the sample after annealing of the Bi_2O_2S

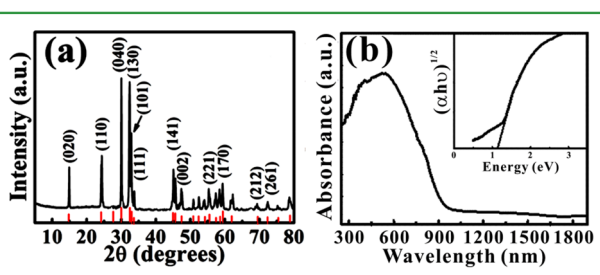

Figure 3. (a) XRD and (b) UV−vis absorbance spectroscopy of Bi_2O_2S nanocrystals.

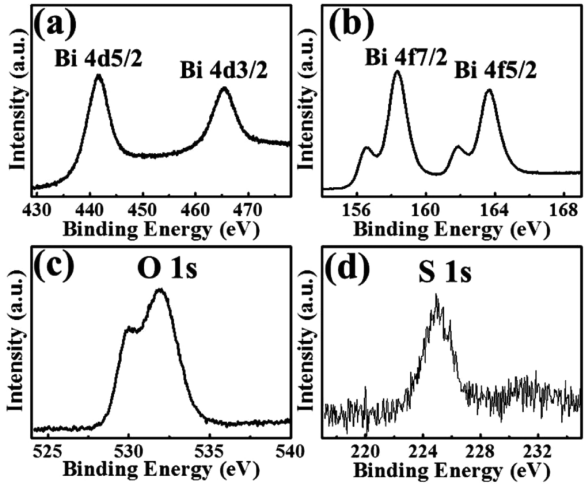

Figure 4. XPS of Bi_2O_2S nanocrystals for (a) Bi 4d, (b) Bi 4f, (c) O1s, and (d) S 1s.

single crystals (Figure S2 in the Supporting Information). Figure 4a−d show the XPS of Bi 4d, Bi 4f, O1s, and S 1s, respectively. There are two narrow and symmetric peaks at 441.3 and 465.1 eV in Figure 4a, corresponding to Bi (III) with a peak splitting of 23.8 eV.[17,23] Figure 4b reveals that Bi 4f have two main peaks at 158.3 and 163.7 eV with a peak split of 5.4 eV from Bi^{3+}.[17] In addition, two shoulder peaks at 156.6 and 161.8 eV arising from the bonding energies of S 2p.[24] Figure 4c indicates that O 1s has bonding energy at 530.1 and 531.9 eV with a peak split of 1.8 eV from O 1s.[17] The binding energy of S 1s (224.9 eV)[24] is shown in Figure 4d.

DOI: 10.1021/am5092159
ACS Appl. Mater. Interfaces 2015, 7, 4442−4448

The semiconductors with an E_g value around 1−1.8 eV are suitable for absorbing most of solar light (UV, visible, and some NIR light). The band gap of Bi_2O_2S (E_g = 1.12 eV) falls in this region. Therefore, photoelectric properties of a Bi_2O_2S sample were measured performed under visible light irradiation lamp at room temperature (Figure 5). The Bi_2O_2S nanocrystals were

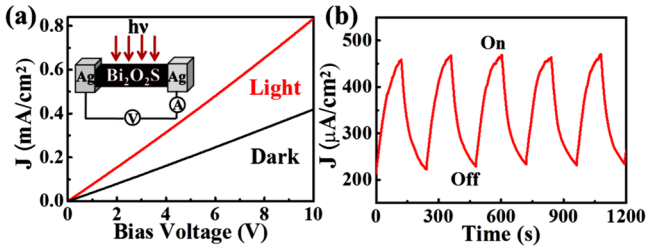

Figure 5. (a) Photoelectric response of Bi_2O_2S nanocrystals and (b) on−off curve at a bias voltage of 6 V.

pressed into ∼1 mm thick film, on which silver paste was dropped to form a sandwich structure (inset in Figure 5). Current−voltage (I−V) curve of Bi_2O_2S nanocrystals film reveals pronounced photovoltaic response compared to the nonirradiated curve. The photocurrent density increased twice of the dark current density from 0.42 to 0.84 mA/cm^2 at the voltage of 10 V, which indicated that Bi_2O_2S nanocrystals possess good photoelectric properties originating from their intense absorption of visible light. On/off photocurrents were measured (Figure 5b) at a bias voltage of 6 V, which reveal two pronounced different states, a low current state and a high current state with the light irradiation on and off. The switching is steady and reversible at an "on" state of 373 μA/cm^2 and "off" state of 253 μA/cm^2, allowing the material to act as a photosensitive switch.

Photoelectric performance of Bi_2O_2S may originate from its crystal and electronic structures. Bi_2O_2S is a layerlike structure but different from BiOCl. Two $[Bi_2O_2]$ layers sandwich S atoms, compared with the Cl species with larger electronnegativity in BiOCl. The electronic structures of these two compounds show that more S 3p orbitals are involved into the valence band maximum (VBM, Bi 6s and S 3p) in Bi_2O_2S than Cl in BiOCl, as shown in Figure 6. Due to the electronnegativity difference between Cl and S, the white bulk binary compound $BiCl_3$ is a wide bandgap material (E_g > 3 eV) but the black bulk Bi_2S_3 has an E_g = 1.3 eV.[14] The excellent photocatalytic property of BiOCl is attributed to the composition of the valence band maximum (VBM, Bi 6s) and the conduction band minimum (CBM, Bi 6p) from the $[Bi_2O_2]$ layers. The band structures and DOS of both BiOCl and Bi_2O_2S are shown in Figure 6. The partial DOS of Cl 3p at the VBM for BiOCl is from the lone-pair electrons of Cl in the van der Waal gaps. The partial DOS analyses of Bi_2O_2S reveal that a large amount of the S (3s, 6p) states are present at the VBM, which are much more than the Bi (6s, 6p) states. The rather widely dispersed Bi 6s and Bi 6p states around the VBM and CBM, seen from the band structure and the density of states (Figure 6b, d), provides high mobility for light-induced e-h separation and transport in photocatalytic property. The calculated E_g values are 3.1 eV for BiOCl and 1.0 eV for Bi_2O_2S from their respective indirect transitions, consistent with the experimental results. Obviously, the S atoms instead of Cl between two $[Bi_2O_2]$ layers narrow the band gap of Bi_2O_2S. The introduction of S columns cause the formation of Bi−S bonds in Bi_2O_2S and each S atom is coordinated to four coplanar Bi atoms. Such coordination of S reduces the coverage of Bi atoms compared with the more spherical coordination of the S in Bi_2S_3 (Figure S3 in the Supporting Information). This fact explains why the E_g of Bi_2S_3 is even wider than that of Bi_2O_2S.

In addition to the unique electronic structures arising from the $[Bi_2O_2]$ layers, the crystal structure of Bi_2O_2S is rather loosely packed. Huang et al. have proposed a simple model based on the crystal packing factor (PF), which is computed by dividing the sum of spherical ion or atom volumes by the unit

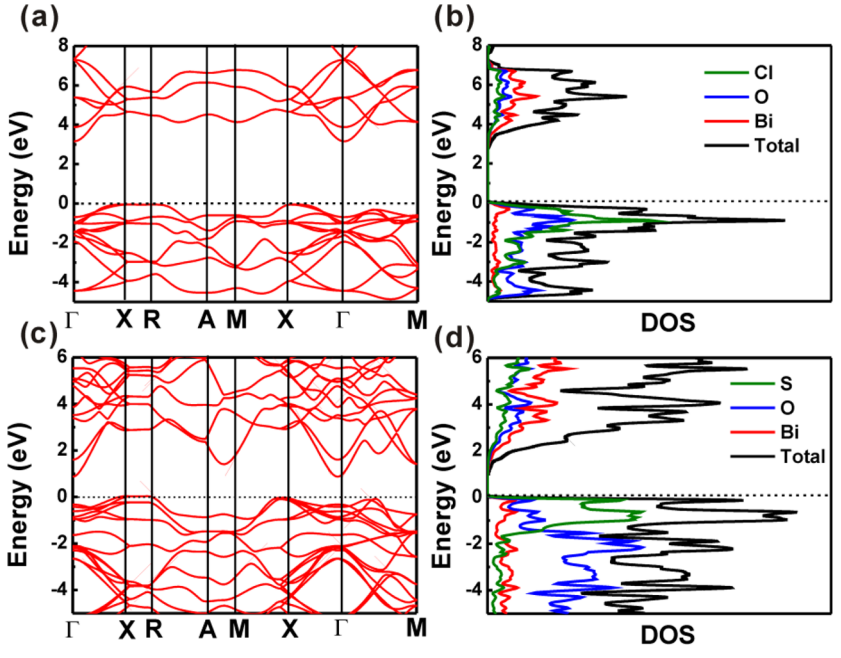

Figure 6. Band structures and DOS of (a, b) BiOCl and (c, d) Bi_2O_2S.

DOI: 10.1021/am5092159
ACS Appl. Mater. Interfaces 2015, 7, 4442−4448

cell volume, to evaluate the charge separation/transport abilities and photoelectric properties of the materials with similar composition or structure.[25−29] The respective PF values of BiOCl and Bi_2O_2S are 0.74 and 0.66. Some well-known photoelectric materials have a low PF value, e.g., 0.65 for anatase TiO_2,[29] 0.66 for multiferroic $BiFeO_3$,[29] 0.56 for multiferroic $KBiFe_2O_5$,[30] and 0.65 for $MAPbI_3$, which are light absorbers in pervoskite-based solar cells. The PF value around 0.65 may be critical for a good light absorber in new-concept solar cells. The concept of packing factor came from Goodenough's idea that lower elastic stiffness can promote distortion, which increases internal field.[31,32] A lower PF structure with lower elastic stiffness possesses higher internal electric field, resulting in more efficient charge separation/transport and thus better photoelectric related properties. In terms of carrier diffusion length, which is associated with the carrier lifetime and mobility, the PF model can provide good explanations on the better properties for looser structure. An open structure (lower PF value) provides wider space for atom vibrations, leading to a higher momentary polarizing field. The more polarizable structure results in larger exciton Bohr radius, hence longer carrier lifetime. In addition, a lower PF structure is usually more deformable, which lowers the hopping barrier for polarons, thus increasing their mobility. The combination of increased carrier lifetime and mobility causes the higher charge separation/transport abilities. Overall, the low-PF Bi_2O_2S may be an excellent photovoltaic material.

When Bi_2O_2S nanocrystals were grounded and pelletized subsequently in the air. Then the samples were vacuum-sealed in evacuated quartz tube and sintered at 500 °C for 6 h to obtain the final samples, the color of the samples changed from deep red to gray (see Figure S4 in the Supporting Information), compared with the reported synthesis from the solid-state reaction of Bi, S and Bi2O3. The $Bi_4O_4S_3$ sample was obtained from the decomposition of the hydrothermally prepared Bi_2O_2S, which should follow the reaction equation below

$$3Bi_2O_2S \rightarrow Bi_4O_4S_3 + 2/3Bi + 2/3Bi_2O_3 \quad (1)$$

This mechanism is supported by the observation of small drops of Bi metal inside the cold end of the quartz tube, which were confirmed by EDX analysis. The presence of Bi_2O_3 nanoparticles were observed to stick to the $Bi_4O_4S_3$ plates, as the SEM and TEM measurements are shown in Figure 7b−d. The X-ray diffraction peaks correspond to those of $Bi_4O_4S_3$ crystallized in the tetragonal structure with space group *I*4/*mmm* but no diffraction peaks of Bi_2O_3 are present, as shown in Figure 7a. Main diffraction peaks of $Bi_4O_4S_3$ at 2θ = 8.6, 13.0, 17.4, 22.4, 25.0, 25.9, 27.2, 30.2, 32.0, 41.6, 48.8, 54.0, and 51.5° correspond to (004), (006), (008), (101), (105), (0012), (107), (109), (110), (1112), (1019), and (1118), planes of the tetragonal $Bi_4O_4S_3$ structure. It is obvious that all Bi_2O_2S crystals have changed to $Bi_4O_4S_3$ after annealing at 500 °C in the evacuated quartz tube. The harvested powder was pressed into pellets, the pellets were sealed in an evacuated silica tube, and the tube was heated for 10 h at 510 °C. The obtained pellets were ground again and the above treatment was repeated. Finally, polycrystalline Bi4O4S3 pellets were obtained.

The crystal structure of $Bi_4O_4S_3$ is shown in Figure 1c, consisting of the rock salt-type Bi_2S_4 layer which was also found in $ROBiS_2$ (R = La, Ce, Gd, and Dy).[10,33−36] There is a more general formula $Bi_4O_4(SO_4)_{1-x}Bi_2S_4$, where x indicates the occupancy of the SO_4 site. There are two stable forms with x = 0 and 0.5, corresponding to $Bi_6O_8S_5$ ($Bi_4O_4(SO_4)Bi_2S_4$) and $Bi_4O_4S_3$ ($Bi_4O_4(SO_4)_{0.5}Bi_2S_4$). The oxidation states of Bi are mixed. Bi atoms in the $[Bi_2O_2]$ layers are +3 due to the regular Bi−O distances (~2.35 Å). Bi atoms in the Bi_2S_4 layers are +2.5, and the mixed valence of Bi may cause superconducting effect. Temperature dependent direct-current (DC) magnetic susceptibility ($M-T$) curve of $Bi_4O_4S_3$ under 10 Oe magnetic field is shown in Figure 7e. Diamagnetic transitions occurred at 4.6 K for both the conditions of zero field cooling (ZFC) and field cooling (FC). The shielding volume fraction at 2 K is about 33%. Figure 7f shows the temperature dependence of resistivity ($\rho-T$) for $Bi_4O_4S_3$. The resistivity decreased rapidly to 0 from 4.6 to 4.1 K, indicating the onset of superconducting transition appeared at 4.6 K. The temperature-dependent resistance, measured under different magnetic field, is depicted in Figure S5 in the Supporting Information. The resistance and the T_c temperature clearly decrease upon the magnetic field is as high as 1 T, indicating a high critical field. However, the resistivity of Bi_2O_2S single crystals exceeds the measuring range of the PPMS instrument from 300 to 2 K. It is obvious that Bi_2O_2S is not superconducting in this temperature range.

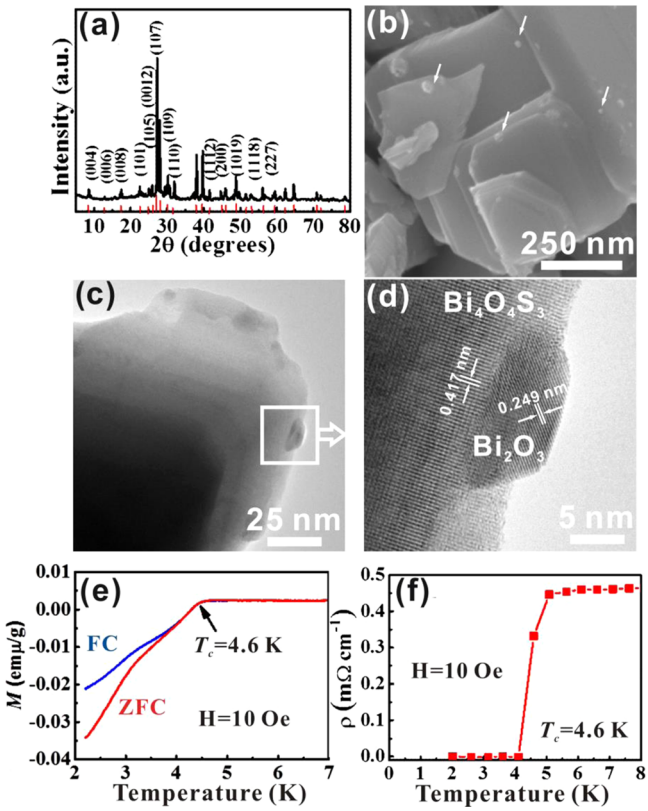

Figure 7. (a) XRD of $Bi_4O_4S_3$. (b) FESEM of $Bi_4O_4S_3$ obtained by annealing the Bi_2O_2S nanocrystals at 500 °C. The arrows indicate the Bi_2O_3 crystals. (c) TEM of $Bi_4O_4S_3$ obtained by annealing the Bi_2O_2S nanocrystals at 500 °C. (d) HRTEM of $Bi_4O_4S_3$ and Bi_2O_3. (e, f) $M-T$ and $R-T$ curve of $Bi_4O_4S_3$.

CONCLUSION

In summary, nanoscale Bi_2O_2S crystals are synthesized via a facile hydrothermal method. Bi_2O_2S nanocrystals show excellent photoelectric properties under the irradiation of visible light at room temperature. First principal calculations and the packing factor model were employed to understand the photoelectric properties of the materials. When Bi_2O_2S

DOI: 10.1021/am5092159
ACS Appl. Mater. Interfaces 2015, 7, 4442−4448

nanocrystals were sintered in an evacuated quartz tube, the color of the samples changed from deep red to black because of the formation of the superconducting $Bi_4O_4S_3$, as confirmed by XRD results. The superconducting transition temperature of $Bi_4O_4S_3$ has been determined to be 4.6 K. The thermal decomposition can provide a feasible route to achieve the conversion of various functional compounds.

■ ASSOCIATED CONTENT

Supporting Information

EDS, XPS, $R-T$ curves of annealed samples. This material is available free of charge via the Internet at http://pubs.acs.org.

■ AUTHOR INFORMATION

Corresponding Authors

*E-mail: huangfq@mail.sic.ac.cn.

*E-mail: huizhang@mail.sic.ac.cn.

Notes

The authors declare no competing financial interest.

■ ACKNOWLEDGMENTS

This work was financially supported by Innovation Program of the CAS (Grant KJCX2-EW-W11), "Strategic Priority Research Program (B)" of the Chinese Academy of Sciences (Grants XDB04040200), NSF of China (Grants 91122034, 51125006, 51202279, 61376056, and 21201012), and Science and Technology Commission of Shanghai (Grant 12XD1406800).

■ REFERENCES

(1) Murata, W.; Onodera, A.; Yoshio, K.; Yamashita, H.; Takama, T. Ferroelectric Phase Transition in Layered Perovskite $SrBi_2Ta_2O_9$. *Ferroelectrics* **2002**, *270*, 303−308.

(2) Zhang, K.-L.; Liu, C.-M.; Huang, F.-Q.; Zheng, C.; Wang, W.-D. Study of the Electronic Structure and Photocatalytic Activity of the BiOCl Photocatalyst. *Appl. Catal., B* **2006**, *68*, 125−129.

(3) Shang, M.; Wang, W.; Zhang, L. Preparation of BiOBr Lamellar Structure with High Photocatalytic Activity by CTAB as Br Source and Template. *J. Hazard. Mater.* **2009**, *167*, 803−809.

(4) Xiao, X.; Zhang, W.-D. Facile Synthesis of Nanostructured BiOI Microspheres with High Visible Light-Induced Photocatalytic Activity. *J. Mater. Chem.* **2010**, *20*, 5866−5870.

(5) Ubaldini, A.; Giannini, E.; Senatore, C.; van der Marel, D. BiOCuS: a New Superconducting Compound with Oxypnictide-Related Structure. *Phys. C* **2010**, *470*, S356−S357.

(6) Mazin, I. Superconductivity and Magnetism in CuBiSO from First Principles. *Phys. Rev. B* **2010**, *81*, 140508.

(7) Shein, I. R.; Ivanovskii, A. L. Electronic Band Structure and Inter-Atomic Bonding in Tetragonal BiOCuS as a Parent Phase for Novel Layered Superconductors. *Solid State Commun.* **2010**, *150*, 640−643.

(8) Mizuguchi, Y.; Fujihisa, H.; Gotoh, Y.; Suzuki, K.; Usui, H.; Kuroki, K.; Demura, S.; Takano, Y.; Izawa, H.; Miura, O. BiS_2-Based Layered Superconductor $Bi_4O_4S_3$. *Phys. Rev. B* **2012**, *86*, 220510.

(9) Singh, S. K.; Kumar, A.; Gahtori, B.; Shruti; Sharma, G.; Patnaik, S.; Awana, V. P. S. Bulk Superconductivity in Bismuth Oxysulfide $Bi_4O_4S_3$. *J. Am. Chem. Soc.* **2012**, *134*, 16504−16507.

(10) Kalai Selvan, G.; Kanagaraj, M.; Esakki Muthu, S.; Jha, R.; Awana, V. P. S.; Arumugam, S. Hydrostatic Pressure Effect on T_c of New BiS_2-Based $Bi_4O_4S_3$ and $NdO_{0.5}F_{0.5}BiS_2$ Layered Superconductors. *Phys. Status Solidi RRL.* **2013**, *7*, 510−513.

(11) Hsu, F. C.; Luo, J. Y.; Yeh, K. W.; Chen, T. K.; Huang, T. W.; Wu, P. M.; Lee, Y. C.; Huang, Y. L.; Chu, Y. Y.; Yan, D. C.; Wu, M. K. Superconductivity in the PbO-Type Structure β-FeSe. *Proc. Natl. Acad. Sci. U. S. A.* **2008**, *105*, 14262−14264.

(12) Zhang, A.-m.; Xia, T.-l.; Liu, K.; Tong, W.; Yang, Z.-r.; Zhang, Q.-m., Superconductivity at 44 K in K Intercalated FeSe System with Excess Fe. *Sci. Rep.* **2013**, *3*.

(13) Dolocan, V. Transmission Spectra of Bismuth Trioxide Thin Films. *Appl. Phys.* **1978**, *16*, 405−407.

(14) Sirimanne, P. M.; Takahashi, K.; Sonoyama, N.; Sakata, T. Photocurrent Enhancement of Wide Bandgap Bi_2O_3 by Bi_2S_3 over Layers. *Sol. Energy Mater. Sol. Cells* **2002**, *73*, 175−187.

(15) Hameed, A.; Montini, T.; Gombac, V.; Fornasiero, P. Surface Phases and Photocatalytic Activity Correlation of Bi_2O_3/Bi_2O_{4-x} Nanocomposite. *J. Am. Chem. Soc.* **2008**, *130*, 9658−9659.

(16) Koyama, E.; Nakai, I.; Nagashima, K. Crystal Chemistry of Oxide-Chalcogenides. II. Synthesis and Crystal Structure of the First Bismuth Oxide-Sulfide, Bi_2O_2S. *Acta Crystallogr., Sect. B* **1984**, *40*, 105−109.

(17) Pacquette, A. L.; Hagiwara, H.; Ishihara, T.; Gewirth, A. A. Fabrication of an Oxysulfide of Bismuth Bi_2O_2S and Its Photocatalytic Activity in a Bi_2O_2S/In_2O_3 Composite. *J. Photochem. Photobiol., A* **2014**, *277*, 27−36.

(18) Lin, X.; Wu, J.; Lu, X.; Shan, Z.; Wang, W.; Huang, F. Novel Antimonate Photocatalysts MSb_2O_6 (M = Ca, Sr and Ba): a Correlation Between Packing Factor and Photocatalytic Activity. *Phys. Chem. Chem. Phys.* **2009**, *11*, 10047−10052.

(19) Blaha, P.; Schwarz, K.; Madsen, G. K. H.; Kvasnicka, D.; Luitz, J. *WIEN2K, An Augmented Plane Wave + Local Orbitals Program for Calculating Crystal Properties*; Technische Universität Wien: Wien, Austria, 2001.

(20) Perdew, J. P.; Burke, K.; Ernzerhof, M. Generalized Gradient Approximation Made Simple. *Phys. Rev. Lett.* **1996**, *77*, 3865−3868.

(21) Blöchl, P. E. Projector Augmented-Wave Method. *Phys. Rev. B* **1994**, *50*, 17953−17979.

(22) Kortüm, G.; Braun, W.; Herzog, G. Principles and Techniques of Diffuse-Reflectance Spectroscopy. *Angew. Chem., Int. Ed. Engl.* **1963**, *2*, 333−341.

(23) Li, R.; Chen, W.; Kobayashi, H.; Ma, C. Platinum-Nanoparticle-Loaded Bismuth Oxide: an Efficient Plasmonic Photocatalyst Active under Visible Light. *Green Chem.* **2010**, *12*, 212−215.

(24) Thomson, J. W.; Cademartiri, L.; MacDonald, M.; Petrov, S.; Calestani, G.; Zhang, P.; Ozin, G. A. Ultrathin Bi_2S_3 Nanowires: Surface and Core Structure at the Cluster-Nanocrystal Transition. *J. Am. Chem. Soc.* **2010**, *132*, 9058−9068.

(25) Wu, J.; Li, J.; Lu, X.; Zhang, L.; Yao, J.; Zhang, F.; Huang, F.; Xu, F. A One-Pot Method to Grow Pyrochlore $H_4Nb_2O_7$-Octahedron-Based Photocatalyst. *J. Mater. Chem.* **2010**, *20*, 1942−1946.

(26) Wu, J.; Huang, F.; Lu, X.; Chen, P.; Wan, D.; Xu, F. Improved Visible-Light Photocatalysis of Nano-$Bi_2Sn_2O_7$ with Dispersed *s*-Bands. *J. Mater. Chem.* **2011**, *21*, 3872−3876.

(27) Wu, J.; Huang, F.; Shan, Z.; Wang, Y. Quasi-Linear Dependence of Cation Filling on the Photocatalysis of A_xBO_3-Based Tunnel Compounds. *Dalton Trans.* **2011**, *40*, 6906−6911.

(28) Yin, X.; Shi, L.; Wei, A.; Wan, D.; Wang, Y.; Huang, F. Effect of Structural Packing on the Luminescence Properties in Tungsten Bronze Compounds $M_2KNb_5O_{15}$ (M=Ca, Sr, Ba). *J. Solid State Chem.* **2012**, *192*, 182−185.

(29) Lü, X.; Yang, W.; Quan, Z.; Lin, T.; Bai, L.; Wang, L.; Huang, F.; Zhao, Y. Enhanced Electron Transport in Nb-Doped TiO_2 Nanoparticles via Pressure-Induced Phase Transitions. *J. Am. Chem. Soc.* **2013**, *136*, 419−426.

(30) Zhang, G.; Wu, H.; Li, G.; Huang, Q.; Yang, C.; Huang, F.; Liao, F.; Lin, J., New high Tc Multiferroics $KBiFe_2O_5$ with Narrow Band Gap and Promising Photovoltaic Effect. *Sci. Rep.* **2013**, *3*.

(31) Goodenough, J.; Menyuk, N.; Dwight, K.; Kafalas, J. Effects of Hydrostatic Pressure and of Jahn-Teller Distortions on the Magnetic Properties of $RbFeF_3$. *Phys. Rev. B* **1970**, *2*, 4640−4645.

(32) Goodenough, J. B.; Zhou, J. S. Localized to Itinerant Electronic Transitions in Transition-Metal Oxides with the Perovskite Structure. *Chem. Mater.* **1998**, *10*, 2980−2993.

(33) Xing, J.; Li, S.; Ding, X.; Yang, H.; Wen, H.-H. Superconductivity Appears in the Vicinity of Semiconducting-Like Behavior in $CeO_{1-x}F_xBiS_2$. *Phys. Rev. B* **2012**, *86*, 214518.

DOI: 10.1021/am5092159
ACS Appl. Mater. Interfaces 2015, 7, 4442−4448

(34) Jha, R.; Kumar, A.; Kumar Singh, S.; Awana, V. P. S. Synthesis and Superconductivity of New BiS_2 Based Superconductor $PrO_{0.5}F_{0.5}BiS_2$. *J. Supercond. Novel Magn.* **2013**, *26*, 499−502.
(35) Li, B.; Xing, Z. W.; Huang, G. Q. Phonon Spectra and Superconductivity of the BiS_2-Based Compounds $LaO_{1-x}F_xBiS_2$. *Europhys. Lett.* **2013**, *101*, 47002.
(36) Lin, X.; Ni, X.; Chen, B.; Xu, X.; Yang, X.; Dai, J.; Li, Y.; Yang, X.; Luo, Y.; Tao, Q.; Cao, G.; Xu, Z. Superconductivity Induced by La Doping in $Sr_{1-x}La_xFBiS_2$. *Phys. Rev. B* **2013**, *87*, 020504.

DOI: 10.1021/am5092159
ACS Appl. Mater. Interfaces 2015, 7, 4442−4448